



Discover Generics

Cost-Effective CT & MRI Contrast Agents

**FRESENIUS
KABI**

[WATCH VIDEO](#)

AJNR

This information is current as
of June 24, 2025.

Diagnostic Performance of Decubitus Photon-Counting Detector CT Myelography for the Detection of CSF-Venous Fistulas







Ajay A. Madhavan, Jeremy K. Cutsforth-Gregory, Waleed Brinjikji, Girish Bathla, John C. Benson, Felix E. Diehn, Laurence J. Eckel, Ian T. Mark, Pearse P. Morris, Melissa A. Payne, Jared T. Verdoorn, Nikkole M. Weber, Lifeng Yu, Francis Baffour, Joel G. Fletcher and Cynthia H. McCollough

AJNR Am J Neuroradiol 2023, 44 (12) 1445-1450

doi: <https://doi.org/10.3174/ajnr.A8040>

<http://www.ajnr.org/content/44/12/1445>

Diagnostic Performance of Decubitus Photon-Counting Detector CT Myelography for the Detection of CSF-Venous Fistulas

 Ajay A. Madhavan,  Jeremy K. Cutsforth-Gregory,  Waleed Brinjikji,  Girish Bathla,  John C. Benson,  Felix E. Diehn,  Laurence J. Eckel,  Ian T. Mark,  Pearce P. Morris, Melissa A. Payne,  Jared T. Verdoorn,  Nikkole M. Weber,  Lifeng Yu,  Francis Baffour,  Joel G. Fletcher, and  Cynthia H. McCollough



ABSTRACT

BACKGROUND AND PURPOSE: CSF-venous fistulas are a common cause of spontaneous intracranial hypotension. Lateral decubitus digital subtraction myelography and CT myelography are the diagnostic imaging standards to identify these fistulas. Photon-counting CT myelography has technological advantages that might improve CSF-venous fistula detection, though no large studies have yet assessed its diagnostic performance. We sought to determine the diagnostic yield of photon-counting detector CT myelography for detection of CSF-venous fistulas in patients with spontaneous intracranial hypotension.

MATERIALS AND METHODS: We retrospectively searched our database for all decubitus photon-counting detector CT myelograms performed at our institution since the introduction of the technique in our practice. Per our institutional workflow, all patients had prior contrast-enhanced brain MR imaging and spine MR imaging showing no extradural CSF. Two neuroradiologists reviewed pre-procedural brain MRIs, assessing previously described findings of intracranial hypotension (Bern score). Additionally, 2 different neuroradiologists assessed each myelogram for a definitive or equivocal CSF-venous fistula. The yield of photon-counting detector CT myelography was calculated and stratified by the Bern score using low-, intermediate-, and high-probability tiers.

RESULTS: Fifty-seven consecutive photon-counting detector CT myelograms in 57 patients were included. A single CSF-venous fistula was definitively present in 38/57 patients. After we stratified by the Bern score, a definitive fistula was seen in 56.0%, 73.3%, and 76.5% of patients with low-, intermediate-, and high-probability brain MR imaging, respectively.

CONCLUSIONS: Decubitus photon-counting detector CT myelography has an excellent diagnostic performance for the detection of CSF-venous fistulas. The yield for patients with intermediate- and high-probability Bern scores is at least as high as previously reported yields of decubitus digital subtraction myelography and CT myelography using energy-integrating detector scanners. The yield for patients with low-probability Bern scores appears to be greater compared with other modalities. Due to the retrospective nature of this study, future prospective work will be needed to compare the sensitivity of photon-counting detector CT myelography with other modalities.

ABBREVIATIONS: CTM = CT myelography; CVF = CSF-venous fistula; DSM = digital subtraction myelography; EID = energy-integrating detector; EVVP = external vertebral venous plexus; IVVP = internal vertebral venous plexus; PC = photon-counting detector; SIH = spontaneous intracranial hypotension; SR = standard resolution; T3D = low-energy threshold; UHR = ultra-high resolution; VMI = virtual monoenergetic image

Spontaneous intracranial hypotension (SIH) is a clinical syndrome caused by a spinal CSF leak. Although the hallmark symptom of SIH is an orthostatic headache, patients may present

with myriad symptoms that are frequently debilitating and occasionally life-threatening. Currently recognized are 3 types of spinal CSF leaks: dural tears (type 1a [ventral tears], type 1b [posterolateral tears]), leaking meningeal diverticula (type 2), and CSF-venous fistulas [CVFs, type 3]).^{1,2} Among these, CVFs are the most recently recognized and most challenging to diagnose.³ Patients with CVFs do not have evidence of extradural CSF on spine imaging (neither MR imaging nor CT myelography [CTM]), because leaked CSF and myelographic contrast are rapidly washed away by draining veins without accumulating in the epidural space. Furthermore, characteristic brain MR imaging abnormalities may be absent in some patients with spinal CSF leaks.⁴ A scoring system (Bern Score) assigning points to various

Received August 22, 2023; accepted after revision September 24.

From the Departments of Radiology (A.A.M., W.B., G.B., J.C.B., F.E.D., L.J.E., I.T.M., P.P.M., J.T.V., N.M.W., L.Y., F.B., J.G.F., C.H.M.), and Neurology (J.K.C.-G., M.A.P.), Mayo Clinic, Rochester, Minnesota.

Drs McCollough and Fletcher receive research support from Siemens Healthineers through a research grant paid to our institution.

Please address correspondence to Ajay Madhavan, MD, Division of Neuroradiology, Department of Radiology, Mayo Clinic, 200 First St SW, Rochester, MN 55905; e-mail: madhavan.ajay@mayo.edu



Indicates article with online supplemental data.

<http://dx.doi.org/10.3174/ajnr.A8040>

brain MR imaging findings was previously shown to predict the probability of finding a spinal CSF leak on myelography, initially being validated in patients with dural tears and subsequently used in the assessment of patients with CVFs.⁵⁻⁷

Digital subtraction myelography (DSM) and CTM are currently the preferred modalities for detecting CVFs at most centers with experience in the diagnosis of spinal CSF leaks, with the latter sometimes being performed in a dynamic (multiphase) fashion.^{8,9} Both modalities have been shown to be effective, especially as techniques for DSM and dynamic CTM have been refined in recent years. In particular, it is now known that performing myelography with the patient in the lateral decubitus position and imaging immediately after intrathecal contrast injection increase the likelihood of detecting CVFs.⁹ Despite many advances, however, neither technique is perfectly sensitive, with some CVFs being missed in patients with clear clinical symptoms of SIH and/or brain MR imaging abnormalities consistent with that diagnosis.^{6,7} Thus, there is a need for continued improvement in imaging techniques to detect CVFs.

In collaboration with another institution, Madhavan et al¹⁰ recently reported a small series of 6 patients in whom CVFs were detected using photon-counting detector CT myelography (PC-CTM). Three of those patients had negative findings on DSM, and 2 had negative findings on dynamic CTM using a conventional energy-integrating detector (EID) CT scanner before the positive findings on PC-CTM. We thus hypothesized that PC-CTM may be an effective technique with a high diagnostic yield for the detection of CVFs. Here, we describe the first large series of patients with SIH studied by PC-CTM, focusing on the diagnostic yield of this examination in patients without extradural CSF on initial spine imaging.

MATERIALS AND METHODS

Patient Selection

This Health Insurance Portability and Accountability Act–compliant retrospective study was approved by our institutional review board. We retrospectively identified all patients who underwent PC-CTM at our institution between February 1, 2023, and June 30, 2023. Clinical information, including indications for the PC-CTM, patient age and sex at the time of the examination, the presence of prior brain and spine MR imaging, and the presence of any prior myelographic studies, were obtained from the medical record. Inclusion criteria were the following: 1) patient meeting the International Classification of Headache Disorders (ICHD-3) criteria for SIH, 2) the presence of at least 1 contrast-enhanced brain MR imaging before PC-CTM, and 3) the absence of spinal extradural fluid on spine MR imaging or conventional CT myelography before PC-CTM. Exclusion criteria were a technically unsuccessful or incomplete PC-CTM or lack of documented consent to use medical information for retrospective research.

Imaging Technique

All PC-CTMs at our institution were performed using the same technique. The patient was placed on the PC-CT scanner (NAEOTOM Alpha; Siemens) in the right lateral decubitus Trendelenburg position. A 20-ga Quincke spinal needle was

advanced into the subarachnoid space at L2–L3 or a lower spinal level under CT guidance. Five milliliters of Omnipaque 300 (GE Healthcare) were injected intrathecally. Low-dose monitoring scans at C7–T1 were performed every 5 seconds to dynamically monitor contrast flow. A series of 3–6 scans of the entire spine was initiated manually when intrathecal contrast reached C7–T1, with the number of scans varying depending on the radiologist's preference and patient-specific factors. All scans were performed during slow inspiration with a 5-second interval between scans. The needle was removed, the patient was rotated to the left lateral decubitus position, and the process was repeated after placing a new spinal needle. Note that a same-day bilateral technique keeping the initial spinal needle in place has been reported, which is likely a viable option for many patients but was not done in this study.¹¹

Among the 3–6 scans in each position, the first 2–4 scans were performed with standard resolution (SR) mode (144 × 0.4 mm detector collimation), and the last 1–2 scans, with ultra-high-resolution (UHR) mode (120 × 0.2 mm detector collimation). The order of SR and UHR scans occasionally varied. All scans had a rotation time of 0.5 seconds and a CARE keV IQ level of 200. Automatic exposure control was used, with a manual tube potential of 140 kV. All scans were reconstructed separately as virtual monoenergetic images (VMIs) at 40 keV and a low-energy threshold (referred to as T3D by the manufacturer and including photon energies from 25 to 140 keV to exclude electronic noise), all with a Br40 kernel (quantum iterative reconstruction strength setting of 3). SR scans were reconstructed at 0.4 mm, and UHR scans were reconstructed at 0.2 mm. Pitch was 1.2 (SR) or 1.0 (UHR), and the approximate time per scan was 5.0 seconds (SR) and 12.0 seconds (UHR).

Imaging Review

For each patient, the most recent pre-PC-CTM brain MR imaging was reviewed by 2 blinded neuroradiologists and assigned a Bern score, which is calculated on the basis of the presence of pachymeningeal enhancement (2 points), venous sinus engorgement (2 points), effacement of the suprasellar cistern of <4 mm (2 points), the presence of subdural fluid collections (1 point), effacement of the prepontine cistern of <5 mm (1 point), and reduction of the mamillopontine distance of <6.5 mm (1 point). Venous sinus engorgement was assessed specifically in the dominant transverse sinus at a paramidline sagittal section on postgadolinium MPRAGE images. Any discrepancy between the 2 reviewers (either in total Bern score or individual components of the score) was resolved by a third adjudicating neuroradiologist.

PC-CTM images were reviewed by 2 neuroradiologists in consensus, both different from the brain MR imaging reviewers. Reviewers specifically assessed the following: 1) the presence or absence of a CVF, 2) whether the CVF was definitive or equivocal, 3) the maximal attenuation of the draining vein, and 4) the scan number on which the finding was first visible. Reviewers were blinded to imaging reports and patient history. Each case was reviewed on a standard PACS workstation capable of generating multiplanar reformats from source axial images. Venous attenuation was determined by placing a circular ROI over the

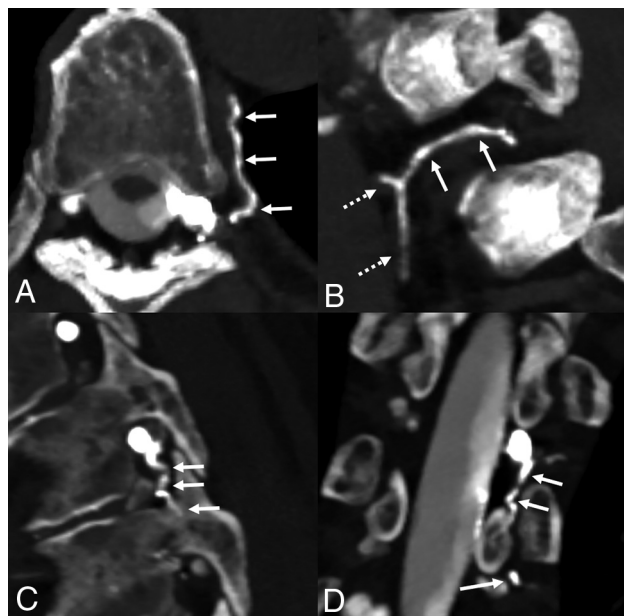


FIG 1. Definitive CVF on PC-CTM involving both the IVVP and EVVP in a patient meeting the ICHD-3 criteria for SIH. Axial MIP images derived from 0.4-mm 40-keV slices demonstrate a left T6 CVF involving the paraspinal segmental vein (A and B, *solid arrows*) and extending into the hemiazygos system (B, *dashed arrows*). Sagittal and coronal 40-keV images (C and D) obtained at a different time point show additional involvement of the IVVP, with contrast extending down to the level of T7 (C and D, *arrows*).

most visually attenuated draining vein on an axial image and reporting the highest value in the ROI. Definitive CVFs had a maximal venous attenuation of >200 HU on T3D images, while equivocal CVFs had a maximal venous attenuation of 100–199 HU on T3D images. These cutoffs were chosen to be at least as stringent as previously proposed Hounsfield unit cutoffs for CVFs, with 1 prior study suggesting a cutoff of 70 HU.¹²

The side and spinal level of the CVF were recorded. Additionally, the most proximal draining vein of each CVF was identified and recorded, specifically noting whether drainage was to the internal vertebral venous plexus (IVVP, medial to the midpoint of the pedicle, *Figs 1–3*) or the external vertebral venous plexus (EVVP, lateral to the midpoint of the pedicle, *Fig 1* and Online Supplemental Data). If no CVF was present, the 2 reviewers also determined whether there was evidence of a type 1 or type 2 leak (dural tear or leaking meningeal diverticulum). Finally, the same 2 neuroradiologists who reviewed the PC-CTMs also reviewed, in consensus, any decubitus DSM or decubitus dynamic EID CTM performed before the PC-CTM, again assessing the presence or absence of a CVF and whether the CVF was definite or equivocal (EID CTMs) or simply whether a definitive CVF was present (DSMs). Only DSMs and EID CTMs that included decubitus positioning and imaging in that same position within 2 minutes of intrathecal contrast injection were included in this review.

The radiation dose of each examination was obtained from the medical record by a single neuroradiologist. Finally, any subsequent treatment based on PC-CTM findings was documented by a single neuroradiologist.¹³

Data Analysis

Mean patient ages and sex distribution were calculated. The mean Bern score of all patients was calculated. The positivity rate (diagnostic yield) of definitive and equivocal CVFs on PC-CTM was calculated and stratified by the Bern score (using previously described low, medium, and high pretest probability tiers). The diagnostic yield of PC-CTM was also stratified by the presence or absence of a previously negative decubitus DSM or decubitus EID CTM.

RESULTS

Patient Characteristics

A total of 63 patients underwent 63 PC-CTMs during the study period. One patient was excluded because she was unable to complete the myelogram secondary to nausea. Five patients were excluded due to lack of documented consent to use medical information for research purposes. Thus, 57 patients having undergone 57 PC-CTMs were included in the final cohort (Online Supplemental Data). Of these, 42 patients were women and 15 were men. The mean age of all patients was 51.2 years (Online Supplemental Data).

Brain MR Imaging Findings

Among the 57 reviewed brain MRIs, there were discrepant findings between the 2 initial reviewers in 2 cases. In the first case, one reviewer noted pachymeningeal enhancement and the other did not. The third adjudicating reviewer deemed pachymeningeal enhancement to be present. In the second case, one reviewer noted venous sinus engorgement and the other did not. The third adjudicating reviewer deemed venous sinus engorgement to be present. There were no other discrepancies among the reported Bern scores (total score or individual components) among the 2 reviewers.

The mean Bern score in the 57 patients was 3.53, with a range of 0–8. Twenty-five of 57 (43.9%) patients had a low-probability Bern score of 0–2, 15/57 (26.3%) patients had an intermediate-probability Bern score of 3–4, and 17/57 (29.8%) patients had a high-probability Bern score of 5–8. No patients had a Bern score of 9.

PC-CTM Findings

A single CVF was identified definitively in 38/57 (66.7%) patients and equivocally in 11/57 (19.3%) patients. No CVF was identified in the remaining 8/57 (14.0%) patients, and none of these 8 patients had a type 1 or 2 leak identified on their PC-CTM. No patients had more than a single CVF. Stratification by Bern score revealed the following:

- 1) In patients with low-probability brain MRIs (Bern score of 0–2, $n = 25$), a single CVF was identified definitively in 14/25 (56.0%) patients and equivocally in 8/25 (32.0%) patients.
- 2) In patients with intermediate-probability brain MRIs (Bern score of 3–4, $n = 15$), a single CVF was identified definitively in 11/15 (73.3%) patients and equivocally in 1/15 (6.7%) patients.
- 3) In patients with a high-probability brain MRI (Bern score of 5–8, $n = 17$), a single CVF was identified definitively in 13/17 (76.5%) patients and equivocally in 2/17 (11.8%) patients.

Definitive CVFs occurred on the right in 25/38 (65.8%) patients and on the left in 13/38 (34.2%) patients, with the most

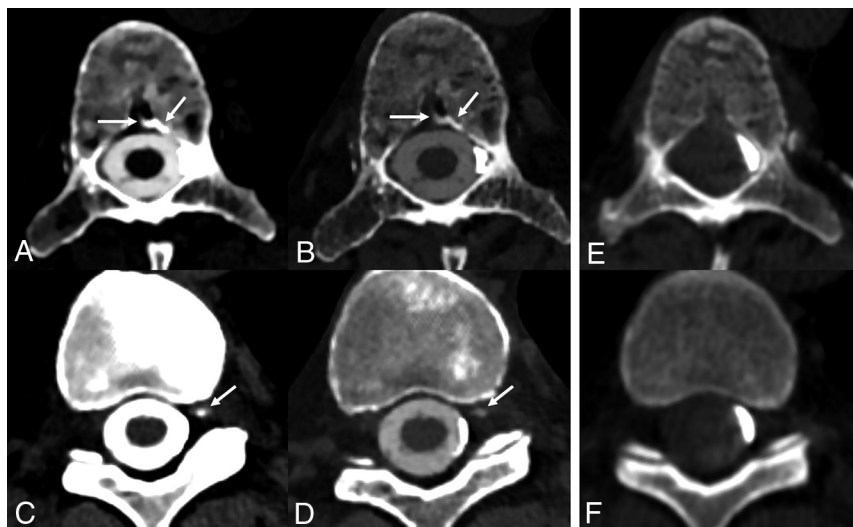


FIG 2. Definitive left T10 CVF involving the ventral IVVP and basivertebral vein in a patient with previously negative findings on decubitus dynamic EID CTM. Axial 40-keV 0.4-mm (A) and T3D 0.2-mm (B) images from PC-CTM, both at the same window/level setting, demonstrate contrast opacification of the T10 basivertebral vein (A and B, arrows), which is most conspicuous on the 40-keV image but defined with better resolution on the T3D image. Axial 40-keV 0.4-mm (C) and T3D 0.2-mm (D) images at the same window/level setting from an adjacent slice at an earlier time point show additional involvement of the ventral IVVP (C and D, arrows). This subtle finding is best seen on the 40-keV image. Neither finding was seen on retrospective review of the patient's dynamic EID CTM (E and F).

frequent spinal level being T10 ($n = 7$, Online Supplemental Data). Equivocal CVFs occurred on the right in 5/11 (46.0%) patients and on the left in 6/11 (54.0%) patients. Regarding venous drainage in the 49 patients with definitive or equivocal CVFs, 17/49 (34.7%) CVFs involved the IVVP only, 28/49 (57.1%) CVFs involved the EVVP only, and 4/49 (8.2%) involved both the IVVP and EVVP. Among the 38 definitive CVFs, 13/38 (34.2%) CVFs involved the IVVP only, 21/38 (55.3%) CVFs involved the EVVP only, and 4/38 (10.5%) involved both the IVVP and EVVP. Among the 38 definitive CVFs, the imaging finding was initially on first scan in 20/38 (52.6%) patients, on the second scan in 5/38 (13.2%) patients, on the fourth scan in 5/38 (13.2%) patients, on the fifth scan in 6/38 (15.8%) patients, and on the sixth scan in 2/38 (5.3%) patients. Among the 11 equivocal CVFs, the imaging finding was seen initially on the first scan in 8/11 (72.7%) patients and on the fifth scan in 3/11 (27.3%) patients. The mean radiation dose (dose-length product) per scan for all included PC-CTMs was 340 mGy-cm. The mean number of scans performed (accounting for both the left and right sides) was 10.

With regard to myelographic studies before PC-CTM, 39/57 (68.4%) patients had a previous DSM. In all cases, this DSM was deemed negative for CVF by both reviewers. On PC-CTM in these patients, a single CVF was identified in 33/39 (84.6%) patients with a negative DSM (Fig 3 and Online Supplemental Data). The CVF was definitive in 22/39 (56.4%) patients and equivocal in 11/39 (28.2%) patients. The mean time interval between DSM and PC-CTM was 57 days, with 15 patients having undergone a nontargeted blood patch between the DSM and PC-CTM.

Eight of 57 (14.0%) patients had undergone a prior decubitus dynamic EID CTM. In all cases, this EID CTM was deemed

negative for CVF by both reviewers. On PC-CTM, a single definitive CVF was identified in 8/8 (100%) patients (Figs 2 and 3 and Online Supplemental Data). The mean time interval between EID CTM and PC-CTM was 30 days, with 4 patients having undergone a nontargeted blood patch between the EID CTM and PC-CTM.

Treatment

All 38 patients with definitive CVFs localized on PC-CTM underwent transvenous Onyx (Medtronic) embolization of the fistula. Among the 11 patients with equivocal CVFs, 6 underwent transvenous Onyx embolization and 5 underwent a targeted transforaminal epidural blood patch. Review of post-treatment images confirmed treatment of the correct spinal level and side.

DISCUSSION

We describe the largest cohort to date of patients with SIH having undergone dynamic decubitus PC-CTM, allowing

several meaningful conclusions. PC-CTM identified a definitive CVF in 66.7% of consecutive patients presenting with SIH in the absence of an extradural CSF. When stratified by the pretest probability of finding a CSF leak on the basis of brain MR imaging Bern score, PC-CTM identified a definitive CVF in 56.0%, 73.3%, and 76.5% of patients with low, intermediate, and high probabilities, respectively. PC-CTM was effective in detecting CVFs draining to the IVVP, EVVP, or a combination of both.

The high diagnostic yield of PC-CTM for detecting CVFs in patients with intermediate and high pretest probability Bern scores is consistent with that in previous studies on decubitus DSM and CTM.^{6,8,9} The yield of PC-CTM in patients with low-probability Bern scores is greater than that reported for other modalities. For example, a prior study on decubitus DSM found that no CVFs were detected in 9 patients with low-probability Bern scores.⁶ Other studies have reported a yield of typically under 20% in patients with low-probability Bern scores when using DSM or EID CTM, though large studies on the yield of EID CTM are lacking.^{4,14} Importantly, we do continue to consider DSM and EID CTM to be excellent modalities for CVF detection. While our findings are interesting, particularly regarding the high yield in patients with low-probability Bern scores, this is a retrospective study with some selection bias, and it does not prove that PC-CTM is more sensitive than DSM or EID CTM. Also, patients with transvenous Onyx embolization may, in particular, be best served with DSM due to extensive streak artifacts caused by Onyx on CT. Many complex factors must be considered because different institutions determine the modalities of choice for CVF detection. Still, our study does provide evidence that PC-CTM has a high yield in patients with SIH and

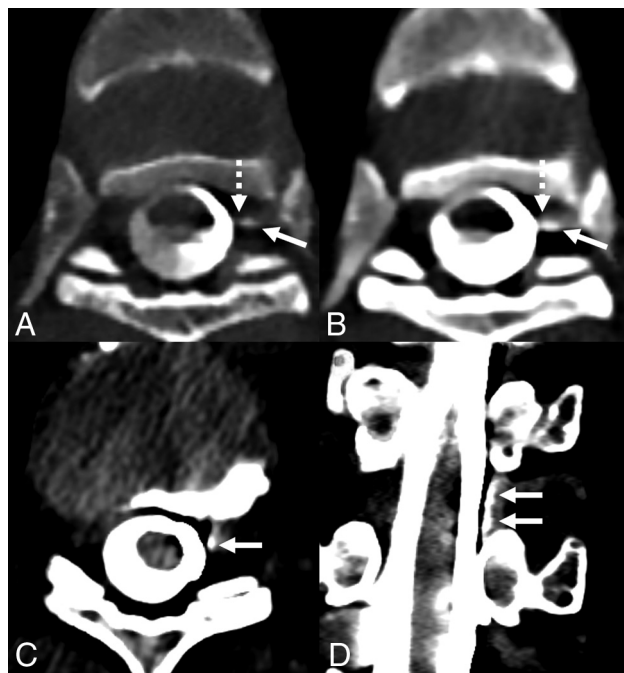


FIG 3. Definitive CVFs involving the IVVP in 2 separate patients, illustrating the complementary benefits of high-spatial-resolution and low kiloelectron volt VMIs. Both patients had a Bern score of 1. The first patient had no prior decubitus myelographic studies, while the second patient initially underwent negative decubitus DSM and negative decubitus EID CTM (not shown). In the first patient (A and B), an axial 0.2-mm T3D image (A) from PC-CTM demonstrates a left T6 CVF involving the IVVP (A, solid arrow). The draining vein is clearly separate from the thecal sac (A, dashed arrow), distinguishing it from a direct epidural leak. Concurrent axial 40-keV VMI reconstructed at the minimum allowed slice thickness of 0.4 mm with identical window/level settings demonstrates higher attenuation of the same finding (B, arrow), but the lower spatial resolution less clearly distinguishes the vein from the thecal sac (B, dashed arrow). In the second patient (C and D), axial (C) and coronal (D) 40-keV 0.4-mm VMIs from PC-CTM demonstrate a left T10 CVF of the IVVP (C and D, arrows). In this case, the 0.4-mm slice thickness was sufficient to distinguish the vein from the thecal sac. In both patients, the venous contrast washed away on subsequently obtained images (not shown).

low Bern scores, which is promising and worthy of further investigation.

PC-CT has many advantages that make it beneficial for the detection of CVFs.^{10,15} First, PC-CT has excellent temporal resolution. In our protocol including 3–6 scans of the spine in each decubitus position, the approximate duration of each scan is 3–5 seconds for SR scans and 10–12 seconds for UHR scans (depending on patient body habitus). The interval between scans is approximately 5 seconds. This permits rapid sampling of multiple time points while maintaining a scan speed that is conducive to minimizing respiratory and other motion artifacts. Second, PC-CT has higher spatial resolution compared with EID CT. The minimum section thickness achieved with PC-CT varies between 0.2 mm with the UHR mode and 0.4 mm with the SR mode. Thin-section imaging is invaluable for detecting contrast within tiny veins, or even a thin column of contrast within a larger vein (Online Supplemental Data). High spatial resolution also helps to distinguish small internal epidural veins from the adjacent thecal

sac or veins adjacent to diverticula (Online Supplemental Data). Our protocol included up to 2 UHR scans and 4 SR scans. Although it would be optimal to perform all 6 scans in the UHR mode, in our experience, this practice resulted in too much reduction in temporal resolution.

Finally, PC-CT has inherent spectral imaging capabilities that allow VMIs to be reconstructed without the need for dual-energy/dual-source techniques. VMIs with a kiloelectron volt closer to the K-edge of iodine have the benefit of increasing the iodine signal, which has been shown to increase the conspicuity of subtle CSF leaks, with the main trade-off being an impaired SNR.^{16,17} We found that VMIs as low as 40 keV retained a visually acceptable SNR while maximizing the iodine signal.¹⁰ Although EID-based techniques such as dual-energy CT can also produce low kiloelectron volt VMIs, dual energy scan modes usually require slower scan speeds compared with PC-CT. In our experience, it is the combination of high spatial resolution, high temporal resolution, and VMIs that allows the detection of the most subtle CVFs (Online Supplemental Data).

Radiation dose is an important concern for all types of myelography. In general, PC-CT has a lower radiation dose compared with EID CT with similar or improved image quality.¹⁸ In our study, the mean dose-length product per scan was 340 mGy-cm, with the mean number of scans being 10. Thus, the dose is certainly not trivial. However, we also found that at least 5 scans were needed to identify the imaging finding in 7 cases of definitive CVF and 3 cases of equivocal CVF, suggesting some added value in multiple scans. In our practice, some proceduralists have recently opted to split the contrast injection over multiple scans and review images between scans so that the examination can be stopped if a definitive CVF is identified. This procedure may be an effective means to limit the radiation dose in the future. Alternatively, if a patient has had a previously negative CTM performed with an early scan (immediately after contrast injection), subsequent CT examinations could, instead, start with a slightly delayed scan of several minutes.

Our study has limitations. First and most important, it was not possible to directly compare PC-CTM with other imaging modalities. Although many patients in our study had previously negative DSMs or EID CTMs and subsequently positive PC-CTMs, there is selection bias in the retrospective study design. Future prospective studies directly comparing PC-CTM, DSM, and EID CTM with consistent examination techniques and close timing between the examinations will be needed. Second, our PC-CTMs were reviewed in consensus rather than independently, due to the complexity of the examinations and subtlety of findings in some cases. Reviewers were also aware that they were viewing a PC-CTM, which could introduce bias. Independent review should be considered in future studies when possible.

Finally, our study did not assess treatment response. The scope of this study was to evaluate the diagnostic performance of PC-CTM for detecting CVFs, and future studies focusing on clinical outcomes after treatment will be needed. This limitation is particularly applicable to the equivocal CVFs in our study, in which treatment response would be helpful to determine whether the radiographic findings were clinically relevant. The efficacy of Onyx embolization and other techniques for CVF treatment has

been demonstrated previously, and response to treatment could help confirm radiographically indeterminate findings.^{19–21} As more patients with indeterminate findings are found, future studies discussing treatment response in this patient population, as well as defining better radiographic criteria for definitive versus equivocal CVFs, will be helpful.

Despite its limitations, this is the first study to assess the diagnostic performance of PC-CTM for the detection of CVFs. PC-CTM has a high diagnostic yield for CVF detection. Its potential advantage over DSM and EID CTM warrants further investigation as PC-CT becomes more widely available.

CONCLUSIONS

We describe the first large cohort of consecutive patients with SIH having undergone PC-CTM, showing that it has a high diagnostic yield for detection of CVFs. This study suggests that the yield of PC-CTM compared with decubitus DSM and EID CTM is at least as high for patients with intermediate and high Bern scores and the yield may be higher in those with low Bern scores.

Disclosure forms provided by the authors are available with the full text and PDF of this article at www.ajnr.org.

REFERENCES

- Schievink WI, Maya MM, Jean-Pierre S, et al. **A classification system of spontaneous spinal CSF leaks.** *Neurology* 2016;87:673–79 [CrossRef Medline](#)
- Callen AL, Timpone VM, Schwertner A, et al. **Algorithmic multimodality approach to diagnosis and treatment of spinal CSF leak and venous fistula in patients with spontaneous intracranial hypotension.** *AJR Am J Roentgenol* 2022;219:292–301 [CrossRef Medline](#)
- Schievink WI, Moser FG, Maya MM. **CSF-venous fistula in spontaneous intracranial hypotension.** *Neurology* 2014;83:472–73 [CrossRef Medline](#)
- Schievink WI, Maya M, Prasad RS, et al. **Spontaneous spinal cerebrospinal fluid-venous fistulas in patients with orthostatic headaches and normal conventional brain and spine imaging.** *Headache* 2021;61:387–91 [CrossRef Medline](#)
- Dobrocky T, Grunder L, Breiding PS, et al. **Assessing spinal cerebrospinal fluid leaks in spontaneous intracranial hypotension with a scoring system based on brain magnetic resonance imaging findings.** *JAMA Neurol* 2019;76:580–87 [CrossRef Medline](#)
- Kim DK, Carr CM, Benson JC, et al. **Diagnostic yield of lateral decubitus digital subtraction myelogram stratified by brain MRI findings.** *Neurology* 2021;96:e1312–18 [CrossRef Medline](#)
- Callen AL, Pattee J, Thaker AA, et al. **Relationship of Bern score, spinal elastance, and opening pressure in patients with spontaneous intracranial hypotension.** *Neurology* 2023;100:e2237–46 [CrossRef Medline](#)
- Kranz PG, Gray L, Amrhein TJ. **Decubitus CT myelography for detecting subtle CSF leaks in spontaneous intracranial hypotension.** *AJNR Am J Neuroradiol* 2019;40:754–56 [CrossRef Medline](#)
- Mamlouk MD, Ochi RP, Jun P, et al. **Decubitus CT myelography for CSF-venous fistulas: a procedural approach.** *AJNR Am J Neuroradiol* 2021;42:32–36 [CrossRef Medline](#)
- Madhavan AA, Yu L, Brinjikji W, et al. **Utility of photon-counting detector CT myelography for the detection of CSF-venous fistulas.** *AJNR Am J Neuroradiol* 2023;44:740–44 [CrossRef Medline](#)
- Carlton Jones L, Goadsby PJ. **Same-day bilateral decubitus CT myelography for detecting CSF-venous fistulas in spontaneous intracranial hypotension.** *AJNR Am J Neuroradiol* 2022;43:645–48 [CrossRef Medline](#)
- Kranz PG, Amrhein TJ, Gray L. **CSF venous fistulas in spontaneous intracranial hypotension: imaging characteristics on dynamic and CT myelography.** *AJR Am J Roentgenol* 2017;209:1360–66 [CrossRef Medline](#)
- Brinjikji W, Savastano LE, Atkinson JLD, et al. **A novel endovascular therapy for CSF hypotension secondary to CSF-venous fistulas.** *AJNR Am J Neuroradiol* 2021;42:882–87 [CrossRef Medline](#)
- D'Antona L, Merchan MA, Vassiliou A, et al. **Clinical presentation, investigation findings, and treatment outcomes of spontaneous intracranial hypotension syndrome: a systematic review and meta-analysis.** *JAMA Neurol* 2021;78:329–37 [CrossRef Medline](#)
- Schwartz FR, Malinzak MD, Amrhein TJ. **Photon-counting computed tomography scan of a cerebrospinal fluid venous fistula.** *JAMA Neurol* 2022;79:628–29 [CrossRef Medline](#)
- Houk JL, Marin DM, Malinzak MD, et al. **Dual energy CT for the identification of CSF-venous fistulas and CSF leaks in spontaneous intracranial hypotension: report of four cases.** *Radiol Case Rep* 2022;17:1824–2 [CrossRef Medline](#)
- Albrecht MH, Vogl TJ, Martin SS, et al. **Review of clinical applications for virtual monoenergetic dual-energy CT.** *Radiology* 2019;293:260–71 [CrossRef Medline](#)
- Marth AA, Marcus RP, Feuerriegel GC, et al. **Photon-counting detector CT versus energy-integrating detector CT of the lumbar spine: comparison of radiation dose and image quality.** *AJR Am J Roentgenol* 2023 Aug 30. [Epub ahead of print] [CrossRef Medline](#)
- Brinjikji W, Garza I, Whealy M, et al. **Clinical and imaging outcomes of cerebrospinal fluid-venous fistula embolization.** *J Neurointerv Surg* 2022;14:953–56 [CrossRef Medline](#)
- Kononov A, Gadzhigaev V, Vinogradov E, et al. **Surgical treatment efficacy of CSF-venous fistulas: systematic review.** *World Neurosurg* 2022;161:91–96 [CrossRef Medline](#)
- Mamlouk MD, Shen PY, Sedrak MF, et al. **CT-guided fibrin glue occlusion of cerebrospinal fluid-venous fistulas.** *Radiology* 2021;299:409–18 [CrossRef Medline](#)